 doi:10.20944/preprints202209.0222.v1

Article

All-polymeric electrode based on PEDOT:PSS for in-vivo neural recording

Gilberto Filho [1]*, Cláudio Júnior [1], Bruno Spinelli [1], Igor Damasceno [2], Felipe Fiuza [1] and Edgard Morya [1]

[1] Edmond and Lily Safra International Institute of Neuroscience (ELS-IINN), Macaíba, Brazil
[2] Federal University of Rio Grande do Norte (UFRN), Natal, Brazil
* Correspondence: gilberto.filho@edu.isd.org.br; Tel.: (+55-8499-655-5414 (G.F.))

Abstract: One of the significant challenges today in the brain-machine interface using invasive methods is the stability of the chronic record. In recent years, polymer-based electrodes have gained notoriety for achieving mechanical strength values close to that of brain tissue, promoting a lower immune response to the implant. In this work, we fabricated fully polymeric electrodes based on PEDOT:PSS for neural recording in Wistar rats. We characterized the electrical properties and both in-vitro and in-vivo functionality of the electrodes. Also, we employed histological processing and microscopical visualization to evaluate tecidual immune response in 7, 14, and 21 days post-implant days. Electrodes with 400-micrometer channels showed a 12dB signal-to-noise ratio. Local field potentials were characterized under two conditions: anesthetized and free-moving. There was a proliferation of microglia to the tissue-electrode interface in the first days, with a decrease after 14 days. Astrocytes also migrated to the interface, but there was no continuous recruitment of these cells in the tissue, showing inflammatory stability at 21 days. The signal was not affected by this inflammatory action, demonstrating that fully polymeric electrodes can be an alternative to prolong the valuable time of neural recordings.

Keywords: PEDOT:PSS; Neural recording; Immune response; BMI;

1. Introduction

One of the significant challenges today in the brain-machine interface using invasive methods is the stability of chronic recording. Invasive microelectrodes are generally used to microstimulate or record brain activity close to neurons [1]. Currently, extracellular recording methods make it possible to obtain two different types of signals - the local field potential (LFPs), which reflects the current of multiple neurons, and the action potential, which reflects the firing of only one neuron [2]. However, the immune response to the implant, which is a foreign body, is considered a primary source of instability and signal loss. This is caused by the proliferation of glial cells at the implant site forming a glial scar that encapsulates the tip of the microelectrode. Ultimately, microelectrodes might become unusable after this process [3,4]. The glia/neuron ratio at the site implanted site is commonly used as a metric to assess biocompatibility. However, due to the system's complexity, such an assessment may not reveal the fundamental need to modify these electrodes [5].

In terms of the materials used, two mechanical properties are considered key - Young's Modulus and flexural stiffness. [6] Although Young's modulus defines the intrinsic properties of a material, flexural stiffness plays a more direct role in determining mechanical incompatibility and, therefore, in the immune response provoked in brain tissue [7]. The materials used in conventional recording electrodes, such as metal, carbon, and silicon, are approximately 8-9 orders of magnitude stiffer than the brain tissue inserted into them. Thus, there is a need to develop more flexible electrodes that try to emulate the properties of the tissue where they will be implanted, not only considering the mechanical properties but also in relation. Polymer-based electrodes are gaining more and more notoriety in research due to an approximation of the brain tissue property as presented [8–12])

Aiming to increase the ability to perform the neural recording for a longer time and in an attempt to approximate the mechanical resistance of the materials used with that of brain

 doi:10.20944/preprints202209.0222.v1

tissue, we carried out the manufacture of flexible microelectrodes based on PEDOT: PSS and built through printed molds through printing 3D, in an attempt to cause minor damage to the tissue where it will be implanted and, in this way, can record electrophysiological signals from the cerebral cortex for a longer time due to a possible reduced immune response to the invading material.

2. Materials and Methods

2.1. Manufacture of all-polymeric electrodes

For the fabrication of the electrodes, 3D printed mold (S3, Sethi) were designed using CAD software (Fusion 360) for intracortical electrodes. The molds were printed with a 0.4 mm nozzle and 1.75 mm ABS filament. Polydimethylsiloxane (PDMS) was obtained by mixing it (95:5%wt) with a catalyst. Then, the PDMS was deposited on the negative mold and left for 24h in an oven (oven model) at 37 C. After 24h, the PDMS was manually removed from the negative mold. PEDOT: PSS-based ink (PH 1000, Clevios) was obtained through the steps previously described by [13], in which PEDOT:PSS was stirred for 6 hours at room temperature and filtered through a syringe filter (0.22 m). The filtered PEDOT:PSS solution was frozen by immersion in liquid nitrogen. The frozen PEDOT: PSS was then placed in a lyophilizer (L101, Liotop) and lyophilized for 72h. PEDOT:PSS nanofibrils were redispersed with a mixture (85:15 v/v) of deionized water and dimethyl sulfoxide (DMSO) (Sigma-Aldrich), followed by mechanical agitation for homogenization. The deposition of the PEDOT:PSS ink was performed manually through a syringe on the PDMS negative mold (400um thick and 200um high for deposition), where after deposition, it was left to dry in an oven at 35 (degrees) C. After that, the electrode tracks were isolated with PDMS (0.4um thick). After isolation, the electrode was placed on an acetate plate to connect the PEDOT:PSS lines with silver ink to the Omnitics direct channels (32 channels, Omnetics 1125). This method manufactured for intracortical recording has four channels (400 m in diameter each) for electrophysiological recording.

2.2. Conductivity Measurement

The electrical conductivity measurement of the PEDOT: PSS ink was performed using the four-probe method according to ASTM-F43-99 [14]. The conductivity measurement was based on the method previously described [13]. The equipment was used for point probe, the contact tips were placed with a spacing of 2 mm, and the following formula of conductivity (σ) was applied:

$$\sigma = \frac{I \times D}{V \times L \times E}, \quad (1)$$

Where I is the current applied to the sample, D is the distance between the two electrodes that will measure the voltage, V is the voltage between the electrodes, L is the width of the sample, and E is the thickness.

2.3. Impedance Measurement

The impedance measurement of the electrode channels was performed using an impedance meter (SIGG II, Falk Minow) at 1 kHz, where the channels were immersed in saline solution (0.9%),and a reference electrode and grounding of the electrode were used in the system. Measurements were performed with signal stabilization after 15 minutes of connecting the measurement system.

2.4. Scanning Electron Microscopy

Images were obtained using a scanning electron microscope (SEM) (Auriga 40, Zeiss), and further analysis was performed using ImageJ software.

 doi:10.20944/preprints202209.0222.v1

2.5. $in - vitro$ Recording

The fully polymeric electrode was used to record electrophysiological signals in vitro in saline solution (0.9%), and the cable was connected to a preamplifier (Plexon Inc., USA) connected to the Omniplex® data acquisition equipment (Plexon Inc., USA). The stimulus was placed in saline solution with the electrode and recorded with an acquisition rate of 1000 Hz. The artificially generated signal was also recorded with the Headstage Tester Unit (HTU) (Omniplex, Plexon inc) with an acquisition rate of 1000 Hz.

The signal-to-noise (SNR) was used to validate the signal quality obtained by the electrode. SNR is defined as the ratio of the power spectral density (PSD) of the signal to the power of the noise. In this way, we record the artificial signal by the HTU and subtract it from the measured signal from the electrode to find our noise. The SNR can be obtained by:

$$SNR_{dB} = 10 \lg 10(\frac{P_{signal}}{P_{noise}}), \tag{2}$$

where P_{signal} is the mean power of the signal and P_{noise} is the mean power of the noise.

2.6. Animal Handling

All experiments described were accepted by the Ethics Committee on the Use of Animals (CEUA), from the Edmond and Lily Safra International Institute of Neurosciences, according to the guidelines of the National Council for Animal Experimentation (CONCEA), under the protocol 01/2022. The animal model used in this study were Wistar rats belonging to the vivarium of the IIN-ELS, which were housed in housing boxes (up to a maximum of 3 animals per box) in the period prior to the procedure. However, after electrode implantation, the animals were kept in insulated boxes with light cycles, adequately monitored, and with free access to water and food.

2.7. Surgical Implantation

Wistar rats were anesthetized with isoflurane inhalation (induction of 0.8-1.5 $lmin^{-}1$ oxygen flow, 4-5% isoflurane; state maintenance with 0.8-1.5 $lmin^{-}1$ oxygen flow, and 2-3% isoflurane). Anesthesia was performed with intramuscular application of Atropine (0.05 mg/kg), Xylazine (3 mg/kg), and intraperitoneal application of Ketamine (70 mg/kg). To confirm that the animal was anesthetized, the paw reflex was evaluated. Gazes moistened with saline (0.9%) were placed over the eyes to prevent them from drying. The animal's temperature was maintained at 37C using a heated bed during the entire surgical procedure. The animal's head was shaved to expose the skin, with subsequent positioning of the stereotaxic and making a cut to access the skull, which was properly sanitized before marking the coordinates by the stereotaxic. Trepanations were performed in the coordinates (1.0:2.5 anteroposterior (AP); 2.8:-4.2 mediolateral (ML) and for the implantation of the electrode 0:2.5 dorsoventral (DV)) to perform the craniotomy. Then, the dura was removed from the window with tweezers. In the next step, the screws were fixed to the skull, with the sequential descent of the fully polymeric electrode array inside the open windows. Finally, an acrylic helmet was made around the electrodes and screws to protect these elements.

2.8. Neural Recordings

Rats were initially sedated with isoflurane inhalation (induction of 0.8-1.5 $lmin^{-}1$ oxygen flow, 4-5%), with subsequent headstage docking. Sequentially, the animals were placed in an acrylic box for recording free behavior, and the cable was connected to a preamplifier (Plexon Inc., USA) connected to the Omniplex® data acquisition equipment (Plexon Inc., USA). Field potentials (LFP) were recorded with an acquisition rate of 1000 Hz, with the rat under the influence of isoflurane for approximately 15 minutes. After the effect of isoflurane, the field potentials (LFP) of the rat in free movement in the box were recorded for 15 minutes with an acquisition rate of 1000 Hz. After the recordings, a bandpass filter

 doi:10.20944/preprints202209.0222.v1

from 0.5 to 40 Hz was passed, and the LFP of each channel was analyzed. The Power density spectrum was calculated for each record, both for the anesthetized animal and the animal in free movement. Data were processed and analyzed using the Python language.

2.9. Euthanasia

The animals were anesthetized and euthanized using the exsanguination technique through intracardiac perfusion using 4% paraformaldehyde (4% PFA; pH 7.2) and with the aid of an extracorporeal perfusion pump. The brain was therefore removed from the skull and placed in a solution containing 4% paraformaldehyde (4% PFA; pH 7.2) and kept at 4ºC for 24 h.

2.10. Histological Analysis

Brain samples were placed in a 30% sucrose solution for 3-4 days. The brains were then covered with Tissue Tek®, frozen in a cryostat (brand cryostat) (cabin and specimen temperature -20C), and sectioned into 50 m coronal slices. The sections were stored in cryoprotectant solution (50% glycerol in PBS), and those considered of interest were washed three times in PBS for 5 minutes with minimal agitation. The tissues were then incubated in 1% PBST (99%PBS + 1%Triton^{TM}X100) at room temperature and minimal agitation for 1 hour and then incubated for a further 1 hour in a 10% goat serum solution (NGS) in 0.3% PBST. Incubation with primary antibodies (Ab) was performed for 72h at 4ºC for primary antibodies to glial fibrillary acidic protein (GFAP obtained in rabbit; 1:500; Z0334, Dako) and the cluster of differentiation 68 (CD68 obtained in mouse, 1:500; MCA341R, Serotec). Therefore, the sections were washed in 0.3% PBST and incubated for 2h30 with the secondary antibodies (Mouse-Alexa Fluor 555nm, 1:1000; brand and Rabbit - Alexa Fluor 488nm, 1:1000) in 10%NGS + 90% 0.3% PBST at room temperature. environment and minimal agitation. Sequentially, sections were washed in PBS for 5 min for three times and subsequently incubated with DAPI (1:1000) in PBS for 10 minutes. Finally, samples were washed with PBS for 5 min for five times and mounted. The slides were stored at 4ºC until the images were acquired.

2.11. Image Acquisition and Analysis

Multichannel images were obtained using a fluorescence microscope (Imager.Z2, Zeiss) (20x objective; UV, FITC, and Texas-red fluorescent filter cubes) using an 8-bit RGB scale with the aid of Stereo Investigator software. The images were analyzed in Python, using the scikit-image library.

3. Results and Discussion

3.1. Fabrication and Characterization of de All-polymer Electrode

The use of 3D printing to manufacture electrodes has become an interesting alternative for the area due to its ease of customization, and low-cost [13]. In this sense, molds were carried out for the manufacture of electrodes from these negative molds intracortical (Figure **??**). PDMS was used as a substrate and insulator in the electrodes due to its ability to be inert (causes a lower immunological reaction) and excellent biocompatibility. PEDOT:PSS, in turn, is commercialized in aqueous form and has been widely used in several areas. In addition, it is commonly used with elastomers to manufacture cardiac and neuronal sensors [15,16], and, in this sense, it was also chosen as a conductive material in this work due to its high degree of biocompatibility. PEDOT:PSS was doped with DMSO to increase its electrical conductivity [17]. Modifications of PEDOT:PSS viscosity was described as one of the ways to produce PEDOT:PSS ink for 3D printing [13].

The PEDOT:PSS:DMSO ink was manually deposited on the PDMS substrate (400 m thick), whose contacts were insulated with PDMS layers (400 m) (Figure 1, a), in which each contact channel has 400 m in diameter (Figure 1,b) . In the model, the layer height and the adhesion of the PEDOT:PSS:DMSO deposition on the PDMS substrate were analyzed using SEM (Scanning Electron Microscopy) since PDMS commonly has

Preprints (www.preprints.org) | NOT PEER-REVIEWED | Posted: 15 September 2022 doi:10.20944/preprints202209.0222.v1

hydrophobic characteristics [18]. A layer height of 10.5 1.2 m was found in the channels deposited in the intracortical model (Figure 1,c). The adhesion obtained on the electrodes was considered satisfactory, demonstrating the ability of the PEDOT:PSS:DMSO ink to adhere to the PDMS surface without any surface treatment and, consequently, making the electrode fabrication less complex. The electrical conductivity of PEDOT:PSS varies according to the method of obtaining and doping methods. Some studies show that PEDOT:PSS doped with DMSO can reach values of up to 1500 S/cm [19], but when removed from the water and 3D printed, the values reach 155 S/cm [13]. The values obtained through the measurement by the four-point method were 137 S/cm for the PEDOT:PSS:DMSO ink. This result is in agreement with other findings in the literature [13,20,21], in which a nozzle of 400 m in diameter was used according to the manufacturing method used and, consequently, the non-orientation of the PEDOT nanofibrils was observed: PSS, thus causing a decrease in conductivity. The electrical resistance values of manually deposited PEDOT:PSS:DMSO were analyzed, and values of 180.7 19.5 were observed. In this context, it is noteworthy that impedance is one of the fundamental characteristics of an electrode used for neural recording and its respective values tend to directly influence the signal-to-noise ratio of the electrode [22]. Impedance values at 1 kHz of 7.4 k were obtained for the electrode with a diameter of 400 m, which demonstrates the excellent applicability of PEDOT:PSS:DMSO as a conductor for neural recording. Other studies showed electrode impedance values using PEDOT:PSS as a conductor that ranged from up to 6.3 k [23] to 19.5 k [24].

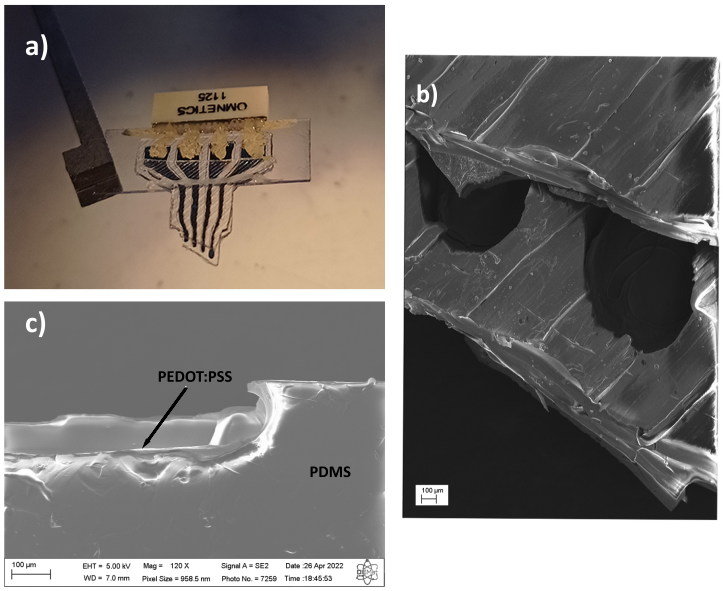

Figure 1. (**a**) Intracortical electrode. (**b**) Image of the intracortical channel obtained with SEM. (**c**) Interface deposition with PEDOT:PSS:DMSO and PDMS, layer deposition of 10.5 1.2 m.

The fully polymeric electrode has four 400 m channels for contact with brain tissue, in which each channel was connected to the omnetics via silver ink lines and insulated with a light-curing resin. Sequentially, at the end of the procedures, the electrodes were weighed on a precision balance, and we obtained weight of 0.5g per prepared, flexible electrode. It was considered that the weight of the complete electrode was within the expected range since manufacturing the fully polymeric electrode was done manually.

3.2. Validation in-vitro

The fully polymeric electrodes were tested with artificial signals to analyze the recording capacity at an acquisition frequency of 1000 Hz. In this sense, all electrode channels

Preprints (www.preprints.org) | NOT PEER-REVIEWED | Posted: 15 September 2022 doi:10.20944/preprints202209.0222.v1

demonstrated excellent ability to record the generated signals and stability over the analysis time. We compared the signal recorded by the electrode with the signal recorded by the Headstage Tester Unit (HTU) equipment, which tests the quality of the signal acquired by the headstage coupled to the plexon system. It was found that both received the same signal and the same acquisition frequency. A bandpass filter (0.5 - 35 Hz) and the calculation of LFP (Figure 2, a and b) and PSD (Figure 2, c) were used to compare whether the signal frequencies were the same. It was possible to verify a difference in the form of the signal recorded by the flexible electrode compared with the signal from the HTU, and, in this context, the characteristics of the material and the form of recording of the electrode are different from that of the HTU. In the HTU, the audio cable is connected directly to the board and in the test with the electrode, it is submerged in saline solution (0.9%) and with a wire transmitting the signal to the solution. From the HTU signal, it is possible to calculate the SNR (Figure 3) in which we use the difference between the signals of the fully polymeric electrode with the HTU and thus, finding an SNR ratio of 12dB, which demonstrates a good signal-to-noise. Studies show that the maximum SNR value at low frequencies (5-30Hz) is approximately 9 dB for Pt and CNTs, and 4 dB for Au [25]. This SNR value demonstrates that the electrode based on PEDOT:PSS:DMSO has interesting applicability for recording low-frequency LFPs.

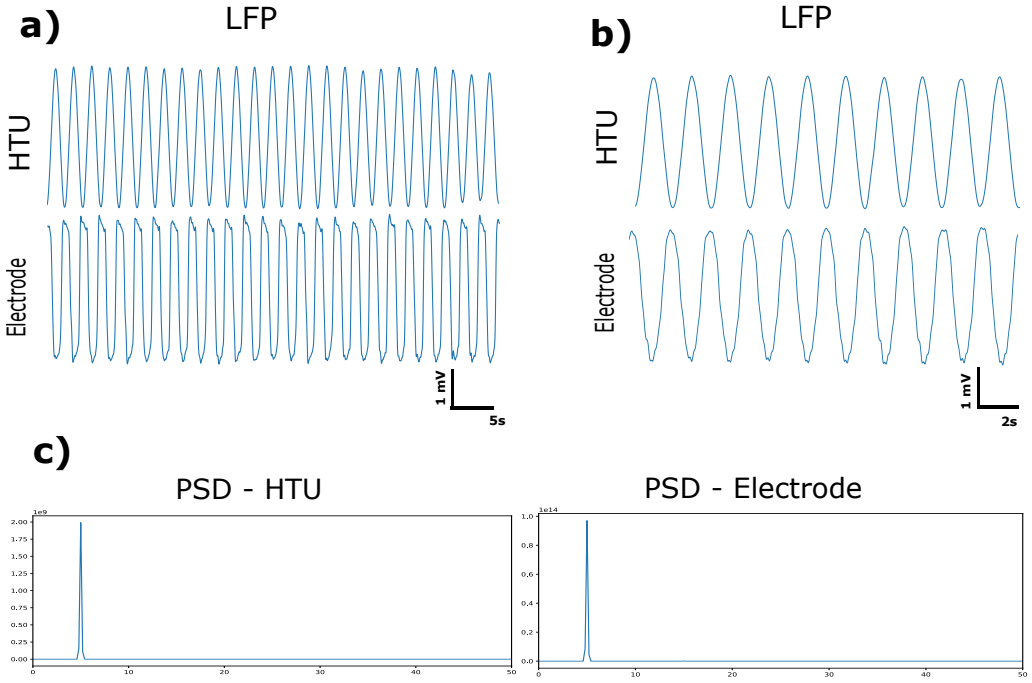

Figure 2. (**a**) Artificial signal LFP with 5s for the HTU and electrode. (**b**) Artificial signal LFP with 2s for the HTU and electrode. (**c**) Artificial signal PSD with the HTU and electrode.

Preprints (www.preprints.org) | NOT PEER-REVIEWED | Posted: 15 September 2022 doi:10.20944/preprints202209.0222.v1

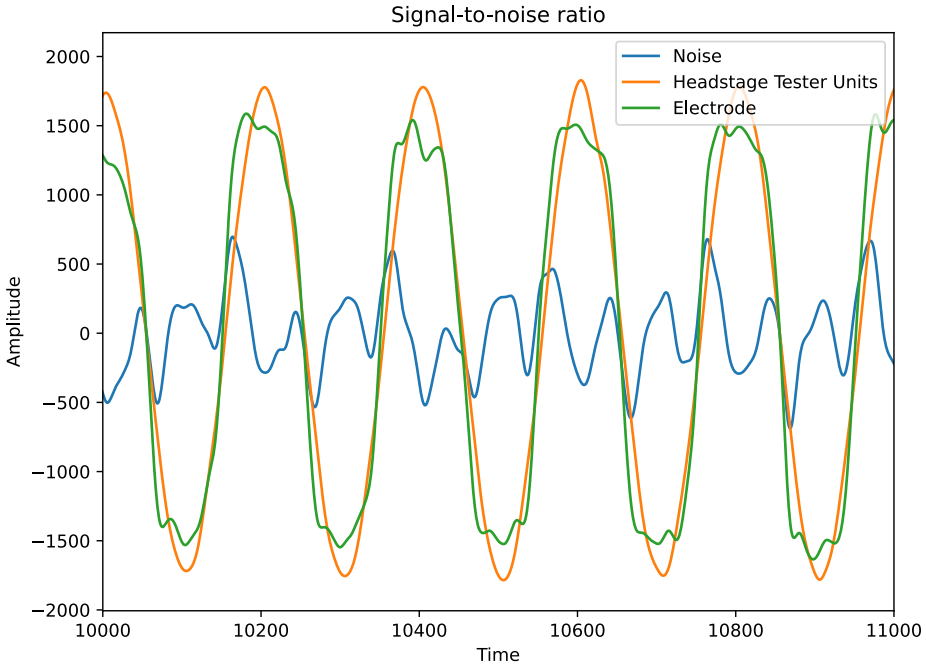

Figure 3. Difference between the signals detected by the HTU, by the electrode and the influence of noise.

3.3. Validation in-vivo

To evaluate the intracortical model of the fully polymeric electrode based on PEDOT:PSS:DMSO, neural recordings were performed in Wistar rats. The electrodes were implanted (Figure 4), focusing on the region of interest of the primary motor cortex (M1), and neuronal activity was recorded at two different times: first, the recording was in an acrylic box with the animal still under the effect of isoflurane anesthesia for 15 minutes. In this state, the animal remained anesthetized and immobile until the anesthetic's effect wore off, so it returned to the awake state. In the second moment, the neuronal recording was performed with the animal in free movement inside the acrylic box. LFPs were recorded at rest at two moments: anesthesia and free movement. To test the ability to long-time recording, animals were recorded at 7, 14, and 21 days after implantation to compare the functionality of the channels as the response to the implant progressed. The data were filtered with a bandpass filter (0.5 - 35 Hz), as the frequencies of interest for recording are contained in this range. We found differences between the LFPs in the conditions where we observed that delta frequencies (0.5 - 4Hz) are more present when the animal is anesthetized with what was in free movement (Figure 5, a), which is in agreement with studies that analyzed the influence of anesthesia on the frequency of neuronal activity [26]. The PSD between states was also calculated, demonstrating the greater intensity of Delta waves in the anesthetized animal compared to the moving animal (Figure 5, b).

Preprints (www.preprints.org) | NOT PEER-REVIEWED | Posted: 15 September 2022 doi:10.20944/preprints202209.0222.v1

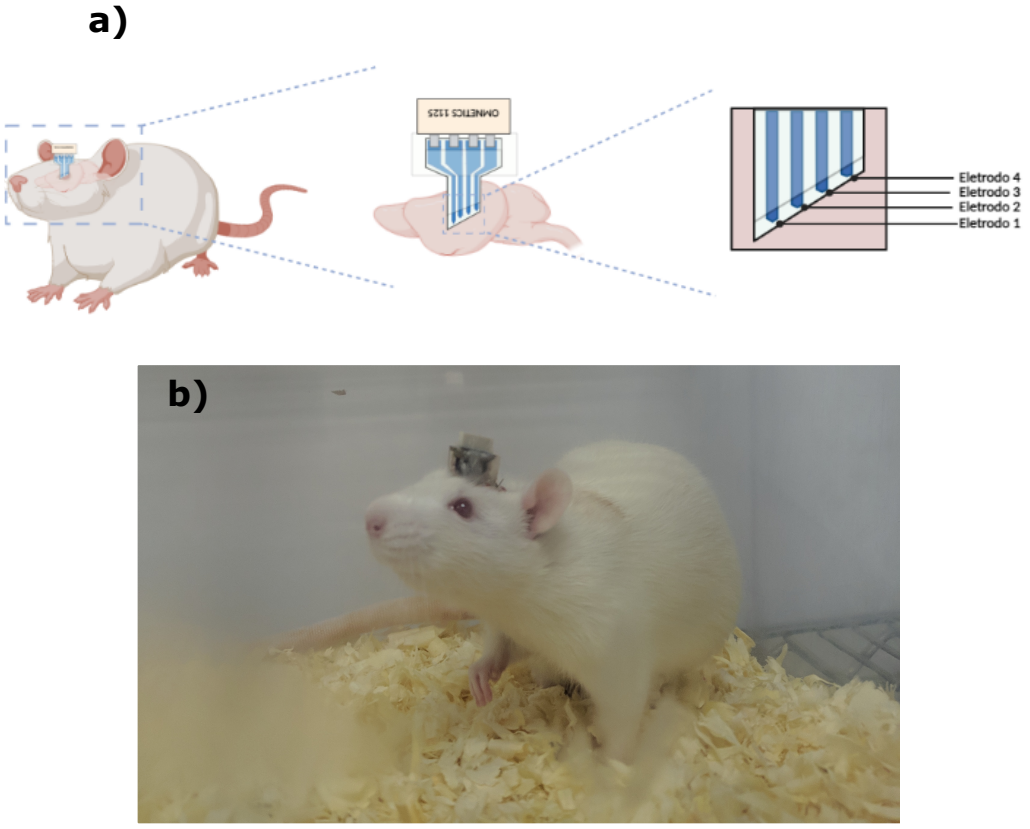

Figure 4. (**a**) Demonstration of the electrode in the rat brain.(**b**) Wistar rat two days after surgery.

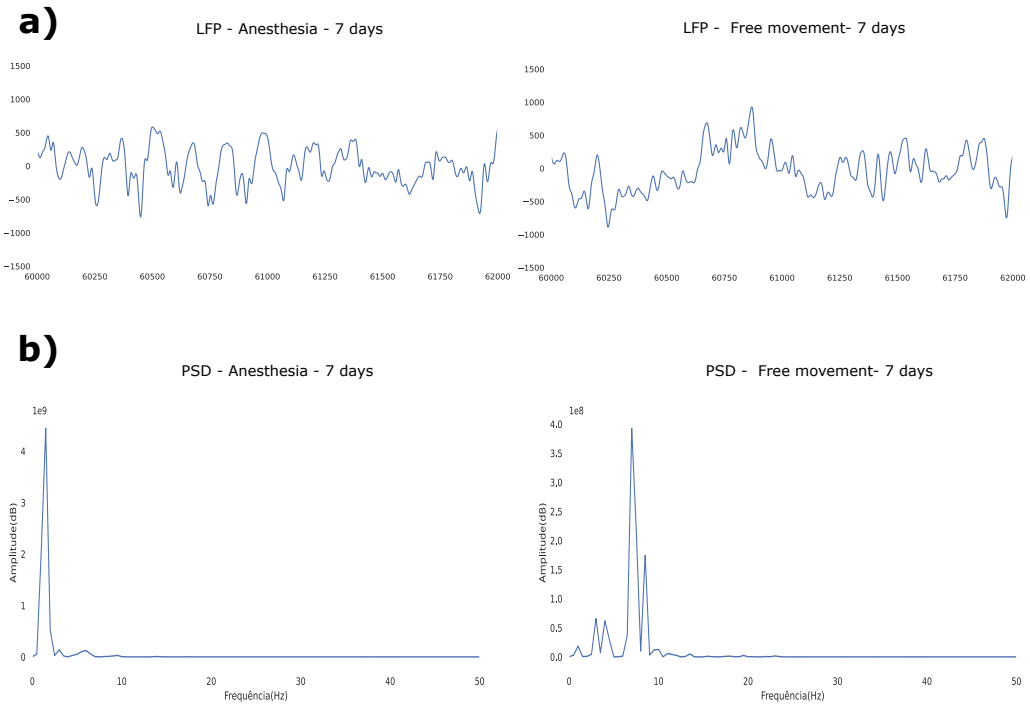

Figure 5. (**a**) LFP between anesthetized and free movement conditions.(**b**) PSD between anesthetized and free movement conditions.

The analysis of the animal in the free movement was performed, in which the spectrogram of the mouse in movement showed changes in frequencies when it performed the movement (Figure 6). Therefore, it was cut to just 1s of motion, and the PSD and

Preprints (www.preprints.org) | NOT PEER-REVIEWED | Posted: 15 September 2022 doi:10.20944/preprints202209.0222.v1

spectrogram were calculated (Figure 7). The frequencies that proved to be predominant were those expected for the M1 region when performing the movement, which is alpha frequencies (8 - 12Hz) [27].

The functionality of the electrode channels over the three weeks was verified with the raw and filtered LFP and the signals were stable after 21 days of surgery and with all functional channels after this period (Figure 8. This result is essential for lead utility issues, as previous studies showed that for PEDOT:PSS-based fully polymeric leads, only 62% of the channels remained functional for two weeks and 45% for four weeks [28].

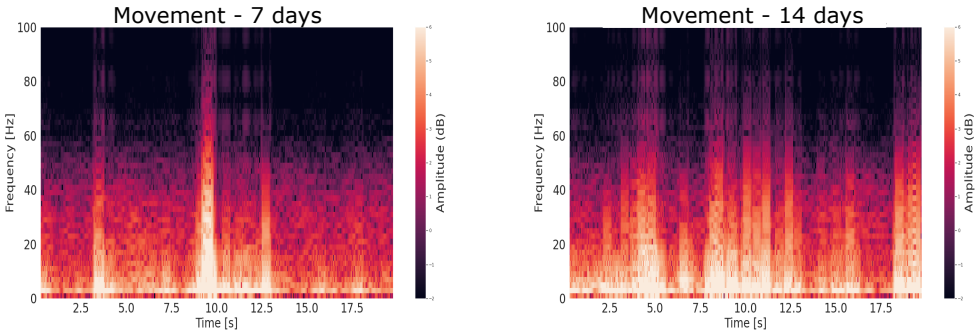

Figure 6. Spectrogram of the moving rat (**a**) 7 days and (**b**) 14 days

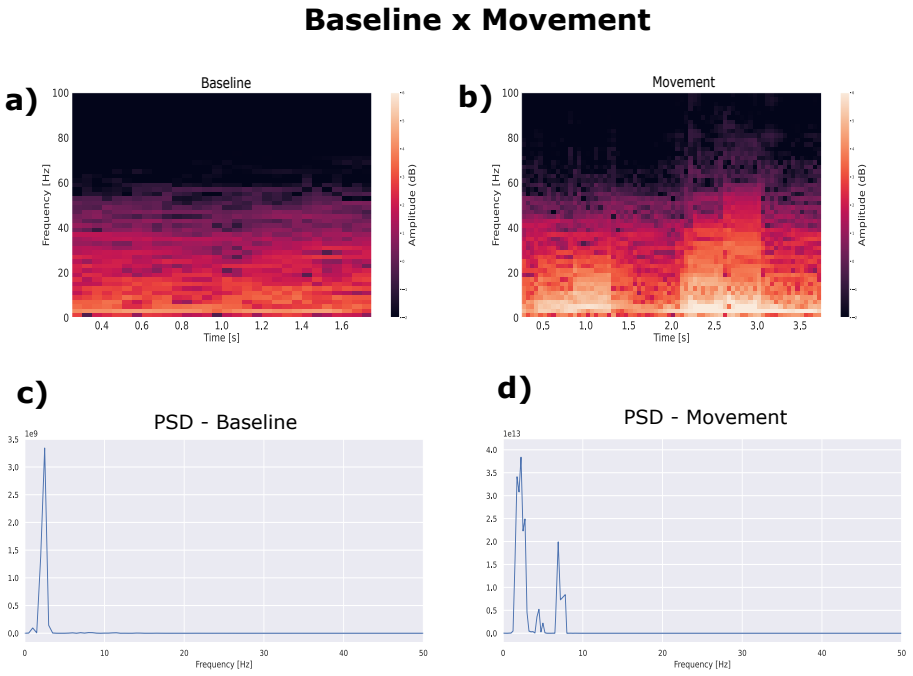

Figure 7. (**a**) Spectrogram of the baseline rat.(**b**) Spectrogram of the moving rat. (**c**) PSD of the baseline rat. (**d**) PSD of the baseline rat in movement.

Preprints (www.preprints.org) | NOT PEER-REVIEWED | Posted: 15 September 2022 doi:10.20944/preprints202209.0222.v1

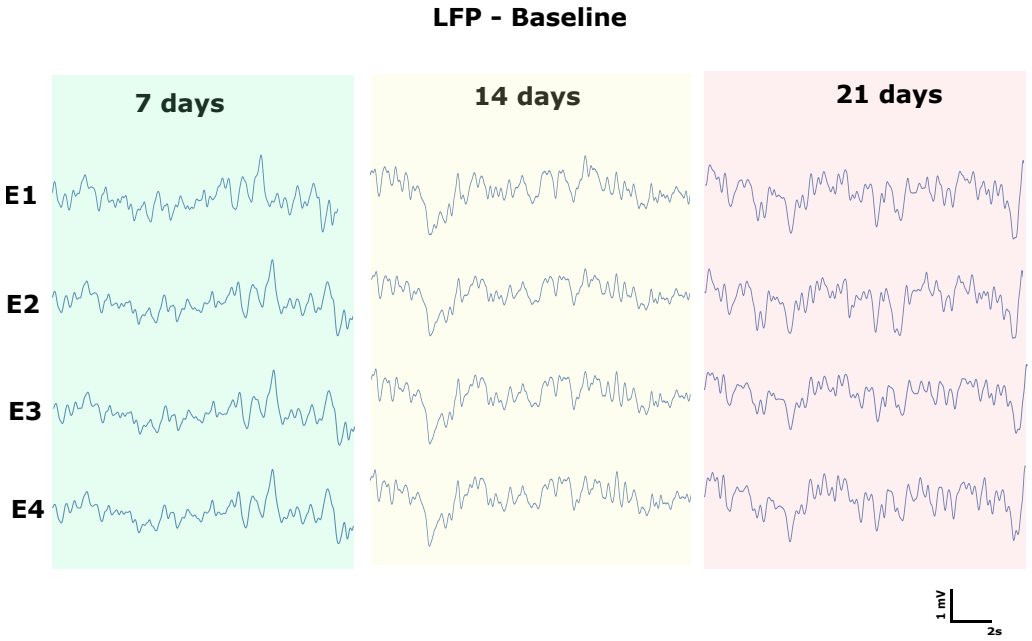

Figure 8. Analysis of functioning and intensity through the LFP of days 7, 14 and 21 of all channels.

3.4. Evolution of the Immune Response

To investigate the evolution of the inflammatory response to the foreign body induced by the intracortical electrode. Electrodes were operated with the same characteristics and in the same region. The immune response evolution was observed at 7, 14, and 21 days after implantation of the fully polymeric electrodes based on PEDOT:PSS:DMSO.

For each rat, brain tissue was sectioned in the coronal plane. The images of the regions which interfaced with the electrode were obtained with different magnifications and were later analyzed using the Scikit-Image library. The images had their pixel intensity normalized; that is, the average vector of the intensity of each image was obtained, and values below the average were zeroed. Then, the interface between the electrode and the tissue was analyzed by lining up a square (1000 m x 1000 m) on each side where the electrode was implanted in the tissue, that is, the left and right interface of the electrodes. Means were calculated for each time and interface (right and left), as well as the intensity of each marker by the distance from the implant site. Images for each time and for each staining provoked by CD68, GFAP, and DAPI were performed to compare the immune response evolution over the days (Figure 9).

 doi:10.20944/preprints202209.0222.v1

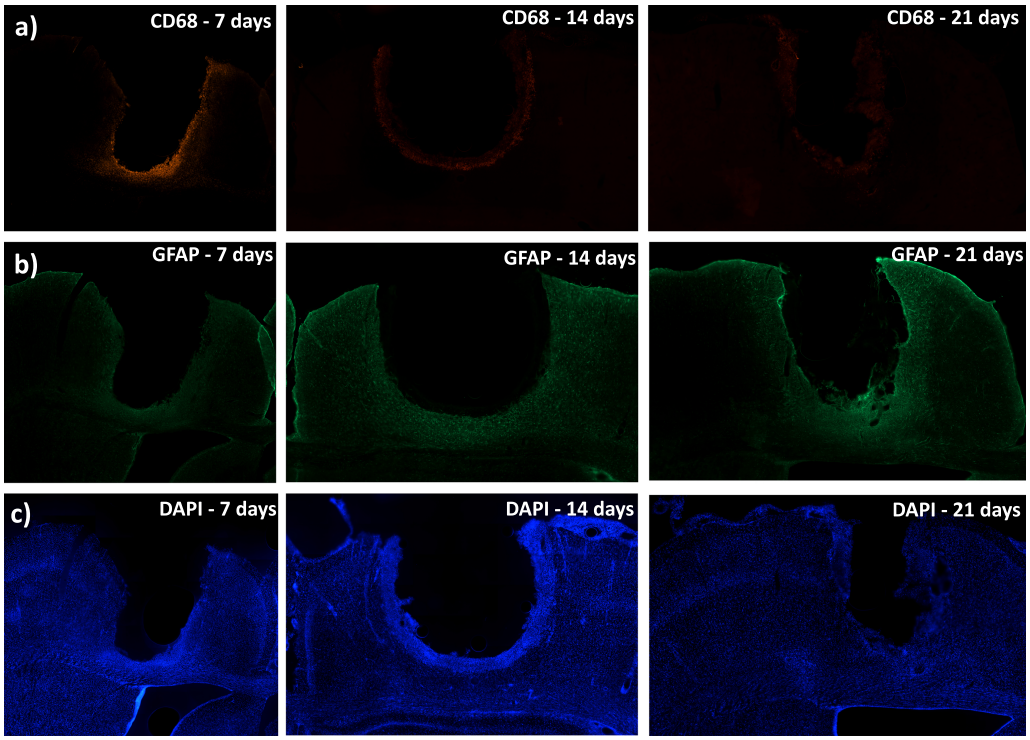

Figure 9. Tissue immune response to implant (**a**) CD68-labeled cells at days 7, 14 and 21. (**b**) GFAP-labeled cells at days 7, 14 and 21. (**c**) DAPI-labeled cells at days 7, 14 and 21 .(

The intensity of each signal was analyzed in different periods, in which the average vector of the intensity was divided by the maximum value in this analyzed square (Figure 10, a, b) and the intensity was verified by the distance of the electrode interface with the tissue (Figure 10, c). CD68 is a marker activated microglia in the nervous system, that is, when there is a proliferation of this type of cell, there will be an increase in the signal intensity of this marker [29]. In this sense, the intensity of the CD68 marker is very apparent in the first 7 days (Figure 10, d), and it is possible to verify a migration of these cells to the interface with the electrode at 14 (Figure 10, e) and 21 days (Figure 10, f). The GFAP marker, which is used to label astrocytes, was also used, and there was an activation of these cells, with migration to the electrode interface at 7 (Figure 11, d) , 14 (Figure 11, e), and 21 (Figure 11, f).

Preprints (www.preprints.org) | NOT PEER-REVIEWED | Posted: 15 September 2022 doi:10.20944/preprints202209.0222.v1

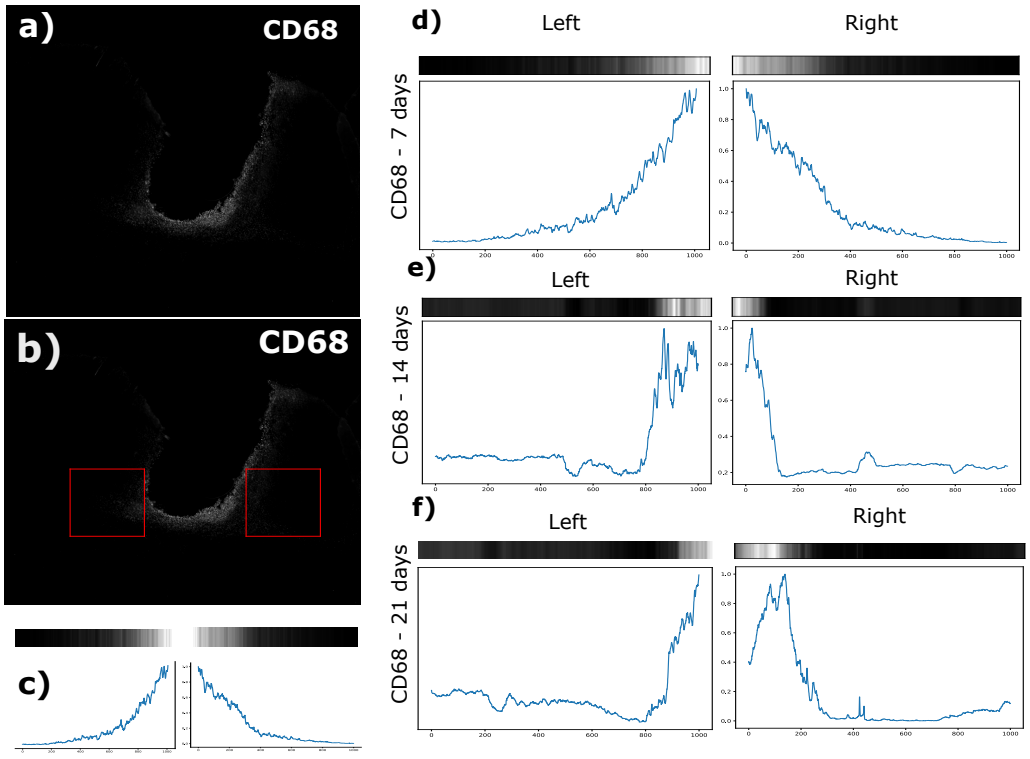

Figure 10. (**a**) Image after treatment with averaging of the intensity vectors. (**b**) Quadrant used to measure CD68 intensity. (**c**) Signal strength near the electrode/tissue interface. (**d**) CD68 signal strength near the electrode/tissue interface for 7 days.(**e**) CD68 signal strength near the electrode/tissue interface for 14 days. (**f**) CD68 signal strength near the electrode/tissue interface for 21 days.(

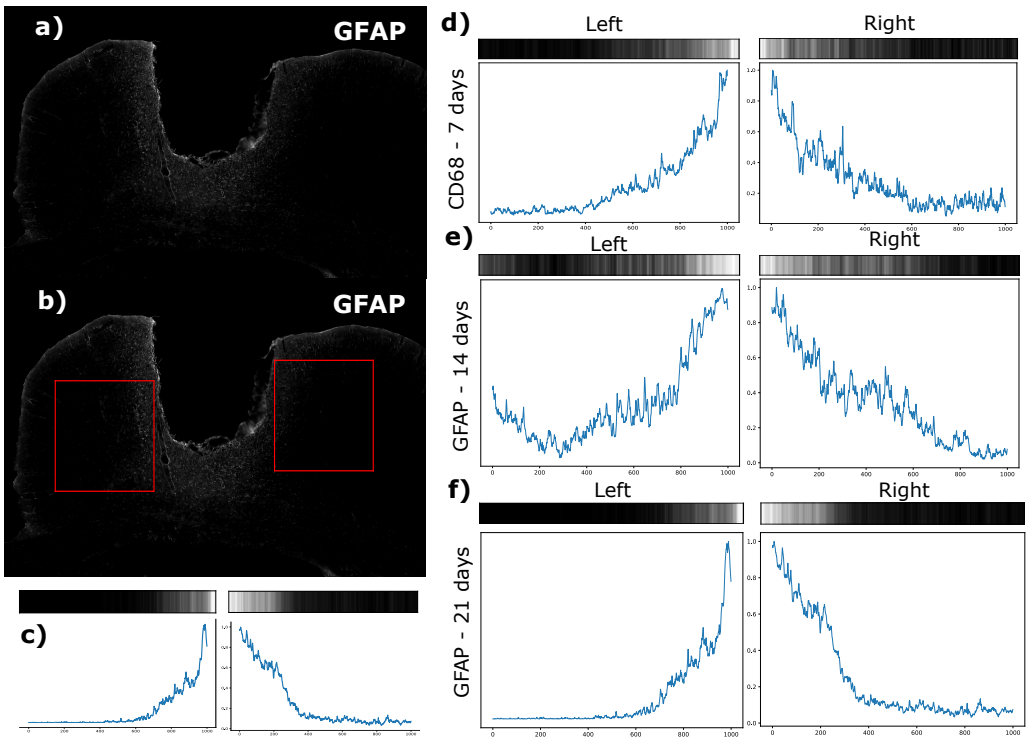

Figure 11. (**a**) Image after treatment with averaging of the intensity vectors. (**b**) Quadrant used to measure GFAP intensity. (**c**) Signal strength near the electrode/tissue interface. (**d**) GFAP signal strength near the electrode/tissue interface for 7 days.(**e**) GFAP signal strength near the electrode/tissue interface for 14 days. (**f**) GFAP signal strength near the electrode/tissue interface for 21 days. (

 doi:10.20944/preprints202209.0222.v1

The average intensity of each image vector relative to the signals was calculated in the selected quadrant and divided by its maximum value. In this way, a graph was obtained in which the intensity of these vectors is related to the distance from the tissue/electrode interface for both sides. It is possible to notice that the CD68 intensity is higher in the first seven days after implantation for a greater distance from the interface, which demonstrates that the recruitment of microglia to the region affected by the electrode lesion occurs initially (Figure 10, d), as shown by other studies [30]. At 14 days, it is possible to verify a higher concentration of microglia at the electrode interface (Figure 10, e), and the characteristic of migration to the interface remains present (Figure 10, f). The GFAP signal intensity tends to increase over the days, showing that in the first 7 days, there is not such a great signal intensity close to the lesion, but a greater distribution occurs as one moves away from the site, with considerable values at 500 m at damage (Figure 11, d). At 14 days, it is also possible to verify an increase in the signal intensity and in the recruitment of astrocytes with a migration to the electrode-tissue interface (Figure 11, e). The intensity of the GFAP signal tends to increase close to the lesion site, and the distance of this intensity decreases as it moves away from the interface, showing that the recruitment of astrocytes decreases considerably (Figure 11, f).

Intensity normalization was performed every day, making the largest value of the vector between the periods become the value at which it would be compared between all. The intensity and distance from the electrode-tissue interface of CD68 tend to be greater (approximately 400 m away) in the initial seven days, as the days of the lesion progress, the intensity tends to decrease, and the proliferation gets closer to the interface (100 m) for days 14 and 21, the latter having the lowest intensity of the 3 (Figure 12). This is typical behavior of microglia, whose primary function is to carry out immune surveillance of the central nervous system through monitoring and response to lesions at the site [31]. In this way, the projection of these microglial cells in the vicinity of the electrode is expected, and they tend to stay at the interface. On the other hand, the intensity of GFAP is opposite to that presented by cells marked by CD68 since GFAP marks astrocytes. GFAP intensity is lower in the first 7 days but with recruitment further away from the lesion. As the days go by, the signal strength tends to increase at 14 and 21 days, but the distance to the signal interface decreases (Figure 12). When tissue damage occurs, astrocytes become reactive, proliferate, and undergo hypertrophy [3]. These have a slower response to damage, but there is migration to the electrode interface [30]. This phenomenon is known as glial scarring, in which the electrode surface undergoes encapsulation and its recording capacity is compromised [30,32].

Preprints (www.preprints.org) | NOT PEER-REVIEWED | Posted: 15 September 2022 doi:10.20944/preprints202209.0222.v1

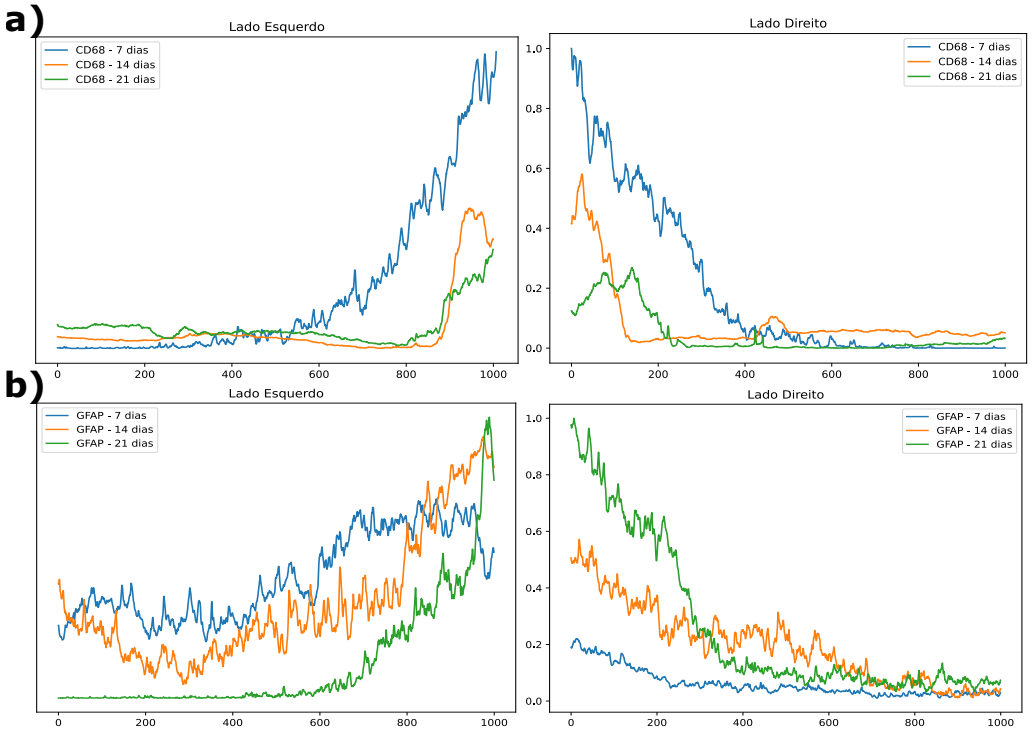

Figure 12. (**a**) Normalized CD68 intensity over 7, 14 and 21 days. (**b**) Normalized GFAP intensity over 7, 14 and 21 days. (

4. Conclusions

The present work demonstrated that using 3D printing to manufacture fully polymeric electrodes based on PEDOT:PSS:DMSO can be an interesting alternative in neural recordings in vivo. The conductive ink based on PEDOT:PSS:DMSO obtained 137 S/cm of electrical conductivity and 180.7 19.5 electrical resistance. Electrodes were obtained with four channels of 400 m in diameter, with an impedance of 7.4 k. The validation of the electrode in vitro demonstrated an SNR of 12dB compared to the HTU, with an attractive signal-to-noise ratio compared to some materials used in electrodes for recording. Neural activity records were performed in Wistar rats from two different conditions to validate the electrode, where it was possible to analyze LFPs from these conditions, demonstrating an ability to perform such a function even in rats in free movement. The immunological response to the electrode was measured using immunohistochemistry with specific markers for cells belonging to the nervous system, CD68, and GFAP for microglia and astrocytes, respectively. We demonstrated that the fully polymeric electrode has an interesting immune response, which is completed around 21 days after implantation, without showing any significant change in the quality of the signal recorded by it.

In general, the fully polymeric electrode based on PEDOT:PSS:DMSO proved to be an effective way to perform neural recording in-vivo, demonstrating an adequate signal-to-noise ratio and good stability over the period studied. The immune response showed that glial encapsulation occurs up to 21 days after implantation without showing any damage to the electrode channels. The next step towards understanding long-term recording properties would be to analyze a more extended period of time, that is, recording for a while more significant than six months and with recording intervals of one or two weeks, in addition to reducing, even more, the size of the electrode. The excellent stability of the device-tissue interface showed to be a promising way to use fully polymeric electrodes in the neural recording.

Author Contributions: Conceptualization, G.F. and E.M.; methodology, G.F., C.J., B.S., I.D., F.F.; software, G.F. and B.S.; formal analysis, G.F. and E.M; investigation, G.F.; resources, G.F. and E.F;

writing—original draft preparation, G.F.; writing—review and editing, G.F. and E.M.; visualization, G.F.; supervision, E.M.; All authors have read and agreed to the published version of the manuscript.

Acknowledgments: This work has been supported by the Brazilian research agency CAPES, and Santos Dumont Institute (ISD).

Conflicts of Interest: The authors declare no conflict of interest.

References

1. Sohal, H.S.; Jackson, A.; Jackson, R.; Clowry, G.J.; Vassilevski, K.; O'Neill, A.; Baker, S.N. The sinusoidal probe: a new approach to improve electrode longevity. *Frontiers in neuroengineering* **2014**, *7*, 10.
2. Buzsáki, G.; Anastassiou, C.A.; Koch, C. The origin of extracellular fields and currents—EEG, ECoG, LFP and spikes. *Nature reviews neuroscience* **2012**, *13*, 407–420.
3. Polikov, V.S.; Tresco, P.A.; Reichert, W.M. Response of brain tissue to chronically implanted neural electrodes. *Journal of neuroscience methods* **2005**, *148*, 1–18.
4. Gulino, M.; Kim, D.; Pané, S.; Santos, S.D.; Pêgo, A.P. Tissue response to neural implants: the use of model systems toward new design solutions of implantable microelectrodes. *Frontiers in neuroscience* **2019**, *13*, 689.
5. Kubota, Y. Untangling GABAergic wiring in the cortical microcircuit. *Current opinion in neurobiology* **2014**, *26*, 7–14.
6. Hong, G.; Lieber, C.M. Novel electrode technologies for neural recordings. *Nature Reviews Neuroscience* **2019**, *20*, 330–345.
7. Chen, R.; Canales, A.; Anikeeva, P. Neural recording and modulation technologies. *Nature Reviews Materials* **2017**, *2*, 1–16.
8. Xie, C.; Liu, J.; Fu, T.M.; Dai, X.; Zhou, W.; Lieber, C.M. Three-dimensional macroporous nanoelectronic networks as minimally invasive brain probes. *Nature materials* **2015**, *14*, 1286–1292.
9. Zhou, T.; Hong, G.; Fu, T.M.; Yang, X.; Schuhmann, T.G.; Viveros, R.D.; Lieber, C.M. Syringe-injectable mesh electronics integrate seamlessly with minimal chronic immune response in the brain. *Proceedings of the National Academy of Sciences* **2017**, *114*, 5894–5899.
10. Hara, S.A.; Kim, B.J.; Kuo, J.T.; Lee, C.D.; Meng, E.; Pikov, V. Long-term stability of intracortical recordings using perforated and arrayed Parylene sheath electrodes. *Journal of neural engineering* **2016**, *13*, 066020.
11. Wei, X.; Luan, L.; Zhao, Z.; Li, X.; Zhu, H.; Potnis, O.; Xie, C. Nanofabricated ultraflexible electrode arrays for high-density intracortical recording. *Advanced Science* **2018**, *5*, 1700625.
12. Kozai, T.D.Y.; Langhals, N.B.; Patel, P.R.; Deng, X.; Zhang, H.; Smith, K.L.; Lahann, J.; Kotov, N.A.; Kipke, D.R. Ultrasmall implantable composite microelectrodes with bioactive surfaces for chronic neural interfaces. *Nature materials* **2012**, *11*, 1065–1073.
13. Yuk, H.; Lu, B.; Lin, S.; Qu, K.; Xu, J.; Luo, J.; Zhao, X. 3D printing of conducting polymers. *Nature communications* **2020**, *11*, 1–8.
14. Girotto, E.M.; Santos, I.A. Medidas de resistividade elétrica DC em sólidos: como efetuálas corretamente. *Química Nova* **2002**, *25*, 639–647.
15. Castrillón, R.; Pérez, J.J.; Andrade-Caicedo, H. Electrical performance of PEDOT: PSS-based textile electrodes for wearable ECG monitoring: a comparative study. *Biomedical engineering online* **2018**, *17*, 1–23.
16. Kozai, T.D.; Catt, K.; Du, Z.; Na, K.; Srivannavit, O.; Razi-ul, M.H.; Seymour, J.; Wise, K.D.; Yoon, E.; Cui, X.T. Chronic in vivo evaluation of PEDOT/CNT for stable neural recordings. *IEEE transactions on biomedical engineering* **2015**, *63*, 111–119.
17. Kim, T.Y.; Kim, J.E.; Suh, K.S. Effects of alcoholic solvents on the conductivity of tosylate-doped poly (3, 4-ethylenedioxythiophene)(PEDOT-OTs). *Polymer international* **2006**, *55*, 80–86.
18. Trantidou, T.; Elani, Y.; Parsons, E.; Ces, O. Hydrophilic surface modification of PDMS for droplet microfluidics using a simple, quick, and robust method via PVA deposition. *Microsystems & nanoengineering* **2017**, *3*, 1–9.
19. Singh, R.; Tharion, J.; Murugan, S.; Kumar, A. ITO-free solution-processed flexible electrochromic devices based on PEDOT: PSS as transparent conducting electrode. *ACS applied materials & interfaces* **2017**, *9*, 19427–19435.
20. Liu, Y.; Liu, J.; Chen, S.; Lei, T.; Kim, Y.; Niu, S.; Wang, H.; Wang, X.; Foudeh, A.M.; Tok, J.B.H.; et al. Soft and elastic hydrogel-based microelectronics for localized low-voltage neuromodulation. *Nature biomedical engineering* **2019**, *3*, 58–68.
21. Wang, Y.; Zhu, C.; Pfattner, R.; Yan, H.; Jin, L.; Chen, S.; Molina-Lopez, F.; Lissel, F.; Liu, J.; Rabiah, N.I.; et al. A highly stretchable, transparent, and conductive polymer. *Science advances* **2017**, *3*, e1602076.
22. Neto, J.P.; Baião, P.; Lopes, G.; Frazão, J.; Nogueira, J.; Fortunato, E.; Barquinha, P.; Kampff, A.R. Does impedance matter when recording spikes with polytrodes? *Frontiers in neuroscience* **2018**, *12*, 715.
23. Liu, Y.; Li, J.; Song, S.; Kang, J.; Tsao, Y.; Chen, S.; Mottini, V.; McConnell, K.; Xu, W.; Zheng, Y.Q.; et al. Morphing electronics enable neuromodulation in growing tissue. *Nature biotechnology* **2020**, *38*, 1031–1036.
24. Garma, L.D.; Ferrari, L.M.; Scognamiglio, P.; Greco, F.; Santoro, F. Inkjet-printed PEDOT: PSS multi-electrode arrays for low-cost in vitro electrophysiology. *Lab on a Chip* **2019**, *19*, 3776–3786.
25. Suarez-Perez, A.; Gabriel, G.; Rebollo, B.; Illa, X.; Guimerà-Brunet, A.; Hernández-Ferrer, J.; Martínez, M.T.; Villa, R.; Sanchez-Vives, M.V. Quantification of signal-to-noise ratio in cerebral cortex recordings using flexible MEAs with co-localized platinum black, carbon nanotubes, and gold electrodes. *Frontiers in neuroscience* **2018**, *12*, 862.
26. Sorrenti, V.; Cecchetto, C.; Maschietto, M.; Fortinguerra, S.; Buriani, A.; Vassanelli, S. Understanding the effects of anesthesia on cortical electrophysiological recordings: a scoping review. *International Journal of Molecular Sciences* **2021**, *22*, 1286.

 doi:10.20944/preprints202209.0222.v1

27. Rickert, J.; de Oliveira, S.C.; Vaadia, E.; Aertsen, A.; Rotter, S.; Mehring, C. Encoding of movement direction in different frequency ranges of motor cortical local field potentials. *Journal of Neuroscience* **2005**, *25*, 8815–8824.
28. Ferlauto, L.; Vagni, P.; Fanelli, A.; Zollinger, E.G.; Monsorno, K.; Paolicelli, R.C.; Ghezzi, D. All-polymeric transient neural probe for prolonged in-vivo electrophysiological recordings. *Biomaterials* **2021**, *274*, 120889.
29. Perego, C.; Fumagalli, S.; De Simoni, M.G. Temporal pattern of expression and colocalization of microglia/macrophage phenotype markers following brain ischemic injury in mice. *Journal of neuroinflammation* **2011**, *8*, 1–20.
30. Campbell, A.; Wu, C. Chronically implanted intracranial electrodes: tissue reaction and electrical changes. *Micromachines* **2018**, *9*, 430.
31. Karumbaiah, L.; Norman, S.E.; Rajan, N.B.; Anand, S.; Saxena, T.; Betancur, M.; Patkar, R.; Bellamkonda, R.V. The upregulation of specific interleukin (IL) receptor antagonists and paradoxical enhancement of neuronal apoptosis due to electrode induced strain and brain micromotion. *Biomaterials* **2012**, *33*, 5983–5996.
32. Kozai, T.D.; Jaquins-Gerstl, A.S.; Vazquez, A.L.; Michael, A.C.; Cui, X.T. Brain tissue responses to neural implants impact signal sensitivity and intervention strategies. *ACS chemical neuroscience* **2015**, *6*, 48–67.